Transient natural convection in a cavity with heat input and a constant temperature wall on opposite sides

Federico Poujol, Jorge Rojas and Eduardo Ramos
Laboratorio de Energía Solar, IIM-UNAM, Temixco, Morelos, Mexico

The transient natural convection of a fluid with Prandtl number of order 200 in a two-dimensional square cavity has been numerically studied. One of the vertical walls of the cavity is kept at a constant (ambient) temperature and a constant heat flux is applied on the opposite wall. The other walls are adiabatic. Initially, a boundary layer is formed near the heated wall; subsequently, a large vortical structure is generated, together with an upper intrusion layer. As time progresses, the average temperature in the cavity increases, and a descending boundary layer is formed near the constant temperature wall. During the transition to the steady-state regime, a thermal stratification pattern is formed. The results are compared with the scale analysis presented by Patterson and Imberger (1980).

Keywords: transient convection; cavity flow

Introduction

Transient natural convection in rectangular enclosures has been studied in an effort to understand the heat transfer properties of systems that are found both in nature and in engineering applications. Although a number of relevant studies have been reported in the literature in the last decade, the phenomenon is far from being properly understood, since it has proved to be extremely complex in nature. The studies have mostly been carried out with symmetric boundary conditions of instantaneous heating and cooling of opposite vertical sidewalls, although this is by no means the only possibility. Patterson and Imberger (1980) presented a scale analysis and established a classification of possible flows in a two-dimensional (2-D) rectangular enclosure in terms of three parameters: Rayleigh number ($Ra_{\Delta T}$), Prandtl number (Pr), and aspect ratio (A). These authors predicted time, length, and velocity scales for the boundary layers in the regions next to the heated and cooled walls as well as for the intrusion layers that result from the discharge of the boundary-layer flows into the cavity. A notable feature predicted is that steady-state conditions can be approached via either monotonic or oscillatory flows, depending on the parameter values.

Numerical solutions of the mass, momentum, and energy-balance equations that govern the flow have been obtained by several authors for a variety of parameter ranges. Most of the flow properties predicted by Patterson and Imberger have been corroborated, and novel detailed features have been discovered. A recent work in this line has been presented by Schladow et al. (1989) who described the following qualitative features. At the early stages, strong thermal gradients are present near the walls, due to the formation of the boundary and intrusion layers. Eventually, a stratified distribution of temperature is achieved in the core with nearly horizontal isotherms. The vertical boundary layers are fed initially through entrainment along their whole vertical extension and then by the horizontal intrusion flows. High- and low-frequency oscillations have been detected as the flow develops; Schladow (1990) has interpreted the high-frequency oscillations that appear in the boundary layers at the early stages in terms of the flow generated by a suddenly heated vertical plate and its instabilities. The oscillating behavior of the flow has been observed and interpreted numerically by Schladow (1990) and numerically and experimentally by Patterson and Armfield (1990). Also, Armfield and Patterson (1991) studied the wave interaction in the system and suggested possible mechanisms for the transition to turbulence. Paolucci and Chenoweth (1989) studied the transition to chaos, and Paolucci (1990) made a direct numerical simulation of the turbulent flow.

A feature of the laminar flow that has received much attention is a flow divergence that appears in the regions near the corners where the boundary layers meet the horizontal walls; its origin has been attributed to a hydraulic jump-like phenomenon. Schladow (1990) criticized this interpretation and suggested that the effect was due to a complex recirculation. Patterson and Armfield (1990) proposed that the discontinuity of the thermal boundary conditions across the corners contributes to the appearance of the divergence. Paolucci and Chenoweth (1989) made 2-D numerical experiments and found that the internal wave instability behavior is consistent with the critical Froude number criteria for internal "hydraulic jumps."

Experimental investigations have confronted enormous difficulties, and consequently misinterpretation and controversy are very difficult to avoid. Experiments have to be designed to comply with initial and boundary conditions that are first devised in the theoretical work. Often trivially imposed initial conditions in theoretical models are extremely difficult to implement experimentally (e.g., instantaneous heating and cooling). Ivey (1984) performed experiments with $Ra = 10^9$, $Pr = 7$, and $A = 1$. Although some qualitative features of the flow were in agreement with the existing predictions, some other features were considerably different. The flow generated by a constant heat input in one of the side walls and a constant

Address reprint requests to Professor Ramos at the Laboratorio de Energía Solar, IIM-UNAM, Ap. P. 34, 62580 Temixco, Morelos, Mexico.

Received 13 January 1992; accepted 26 January 1993

(cold) temperature on the other was also observed by Yewell et al. (1982). Their observations did not show evidence of oscillations, pointing out a discrepancy with the Patterson and Imberger theory. Patterson (1984) clarified the point by demonstrating that the experiments were conducted in a nonoscillatory regime. Patterson and Armfield (1990) carefully matched experimental conditions to those assumed in their theoretical model for $Ra = 3.26 \times 10^8$ and $Pr = 7.5$. They explained a number of flow features and achieved satisfactory agreement between experimental observations and numerical analysis.

In the present investigation, the problem of the transient natural convection in a rectangular cavity is studied using a numerical approach. The initial and boundary conditions differ from those reviewed above. A constant heat flux is instantaneously applied to the system through a vertical wall at the onset of the simulation, while the opposite wall is maintained at a constant temperature equal to the ambient one. The average temperature of the fluid inside the cavity rises monotonically and, eventually, the heat leaves the cavity through the constant-temperature wall, generating a steady-state flow.

Numerical Model

The problem under study is the natural convective flow inside a 2-D square cavity filled with an incompressible Newtonian fluid. The horizontal walls of the cavity are adiabatic and the left-hand-side vertical wall is kept at a constant ambient temperature T'_0. A constant heat flux q is applied at the right-hand-side vertical wall at times $t' = 0$ and maintained thereafter. A schematic representation of the cavity and the coordinate system is presented in Figure 1. The spatial coordinates x' and y' are scaled with the height of the cavity h and the corresponding velocity components u' and v' with the magnitude v/h, where v is the kinematic viscosity of the fluid.

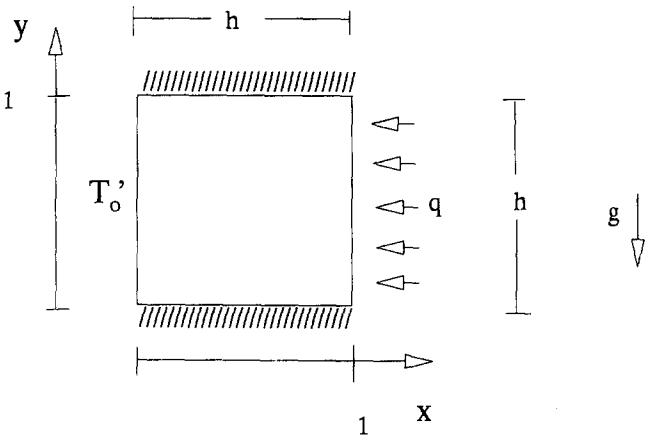

Figure 1 Schematic representation of the cavity

Time is scaled with h^2/v, the pressure with $\rho_o v^2/h^2$, where ρ_o is the density of the fluid at temperature T'_0. The nondimensional temperature is defined as $T = (T' - T'_0)/qh/k$, where k is the thermal conductivity of the fluid.

Using the Boussinesq approximation and expressing the density as a linear function of the temperature, the nondimensional governing equations can be expressed as follows:

Mass balance

$$\frac{\partial u}{\partial x} + \frac{\partial v}{\partial y} = 0 \tag{1}$$

Momentum balance in the x- and y-directions

$$\frac{\partial u}{\partial t} + u\frac{\partial u}{\partial x} + v\frac{\partial u}{\partial y} = -\frac{\partial p}{\partial x} + \frac{\partial^2 u}{\partial x^2} + \frac{\partial^2 u}{\partial y^2} \tag{2}$$

$$\frac{\partial v}{\partial t} + u\frac{\partial v}{\partial x} + v\frac{\partial v}{\partial y} = -\frac{\partial p}{\partial y} + \frac{\partial^2 v}{\partial x^2} + \frac{\partial^2 v}{\partial y^2} + \frac{\mathrm{Ra}}{\mathrm{Pr}} T \tag{3}$$

Notation

g Gravitational acceleration
h Height of the cavity
k Thermal conductivity
p Nondimensional pressure $= \dfrac{p'}{\rho_0 v^2/h^2}$
p' Dimensional pressure
Pr Prandtl number
q Heat flux
Ra Rayleigh number defined in terms of the heat flux
$\mathrm{Ra}_{\Delta T}$ Rayleigh number defined in terms of the temperature difference
T Nondimensional fluid temperature $= \dfrac{T' - T'_0}{qh/k}$
T' Dimensional fluid temperature
T'_0 Dimensional ambient and initial temperature
ΔT^* Characteristic temperature difference near the heated wall
t Nondimensional time $= \dfrac{t'}{h^2/v}$
t' Dimensional time
u Nondimensional velocity component in the x-direction $= \dfrac{u'}{v/h}$
u' Dimensional velocity component in the x-direction
V_T Velocity scale in the thermal boundary layer
v Nondimensional velocity component in the y-direction $= \dfrac{v'}{v/h}$
v' Dimensional velocity component in the y-direction
x Nondimensional spatial coordinate $= \dfrac{x'}{h}$
x' Spatial coordinate
y Nondimensional spatial coordinate $= \dfrac{y'}{h}$
y' Spatial coordinate

Greek symbols

α Thermal diffusivity
β Thermal expansion coefficient
δ_v Thickness of viscous boundary layer
δ_T Thickness of thermal boundary layer
Δ_T Thickness of the intrusion layer
v Kinematic viscosity
ρ_o Reference value of density (initial value)
τ Time scale for the formation of the boundary layer
τ_f Filling time
τ_v Time of arrival of the intrusion layer at the constant-temperature wall

Energy balance

$$\frac{\partial T}{\partial t} + u\frac{\partial T}{\partial x} + v\frac{\partial T}{\partial y} = \frac{1}{\mathrm{Pr}}\left(\frac{\partial^2 T}{\partial x^2} + \frac{\partial^2 T}{\partial y^2}\right) \tag{4}$$

The relevant nondimensional parameters are the Prandtl number

$$\mathrm{Pr} = \nu/\alpha$$

and the Rayleigh number as defined by the expression

$$\mathrm{Ra} = \frac{g\beta q h^4}{k\nu\alpha}$$

where β, g, and α are the volumetric expansion coefficient, the acceleration due to gravity, and the thermal diffusivity, respectively. It must be noted that the definition of the Rayleigh number differs from that used in the scale analysis of Patterson and Imberger (PI) by a factor of $\Delta T/(qh/k)$. When the PI analysis is used, the numerical values of the limits will be modified accordingly (see Appendix).

The initial and boundary conditions considered are

$$u(x, y, 0) = v(x, y, 0) = 0 \quad \text{for} \quad 0 \le x \le 1 \quad 0 \le y \le 1$$
$$T(x, y, 0) = 0 \quad \text{for} \quad 0 \le x \le 1 \quad 0 \le y \le 1$$
$$u(x, 0, t) = v(x, 0, t) = 0 \quad \text{for} \quad 0 \le x \le 1 \quad t \ge 0$$
$$u(x, 1, t) = v(x, 1, t) = 0 \quad \text{for} \quad 0 \le x \le 1 \quad t \ge 0$$
$$u(0, y, t) = v(0, y, t) = 0 \quad \text{for} \quad 0 \le y \le 1 \quad t \ge 0$$
$$u(1, y, t) = v(1, y, t) = 0 \quad \text{for} \quad 0 \le y \le 1 \quad t \ge 0$$
$$T(0, y, t) = 0 \quad \text{for} \quad 0 \le y \le 1 \quad t \ge 0$$
$$\partial T(1, y, t)/\partial x = -1 \quad \text{for} \quad 0 \le y \le 1 \quad t \ge 0$$
$$\partial T(x, 0, t)/\partial y = \partial T(x, 1, t)/\partial y = 0 \quad \text{for} \quad 0 \le x \le 1 \quad t \ge 0$$

The model has been presented in nondimensional form for the sake of generality, although the system of equations is actually solved using a primitive, dimensional variables formulation. A cavity size of 13 cm by 13 cm was considered, and the physical properties of the working fluid were those corresponding to Silicon Oil with 20 centistokes kinematic viscosity. The numerical solution was obtained using the PHOENICS code, which is based on a method similar to the SIMPLE algorithm discussed by Patankar (1989).

A grid-refinement study was carried out to obtain a grid-independent solution. The program was run using grids with 41 × 41, 81 × 81, and 101 × 101 control volumes. The volumes were unevenly distributed according to a quadratic function, in order to have higher spatial resolution near the walls. In Figure 2a, the temperature and vertical velocity are shown as functions of the horizontal coordinate and $y = 0.5$. The data in this figure were obtained at $t = 6.5 \times 10^{-2}$ non-dimensional time units when the boundary layers have already been established. The temperature and the horizontal velocity as functions of the vertical coordinate for $x = 0.5$ and $t = 0.16$ are shown in Figure 2b; at this stage, the "nose" of the intrusion layer has passed the point $x = 0.5$. The qualitative behavior for all cases is the same, and the results obtained with the 101 × 101 and 81 × 81 are almost equal. The maximum difference between the coarser and the finer grids is 10 percent in the velocity and 2 percent in the temperature, in most cases the difference was significantly smaller. All the results reported in this study were obtained with the 81 × 81 grid. The time step used in the integration is 1.4×10^{-3}. This value was considered satisfactory, since further refinement to 3×10^{-4} yielded results that differed by less than 4 percent. It was

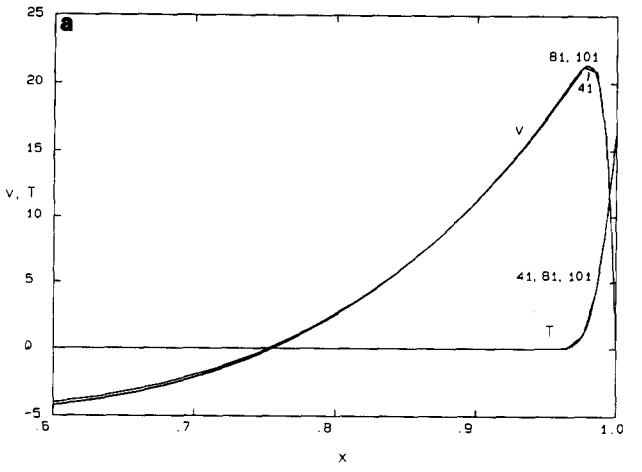

Figure 2a Vertical component of the velocity (v) and temperature (T) as functions of x for $y = 0.5$ and $t = 6.5 \times 10^{-2}$

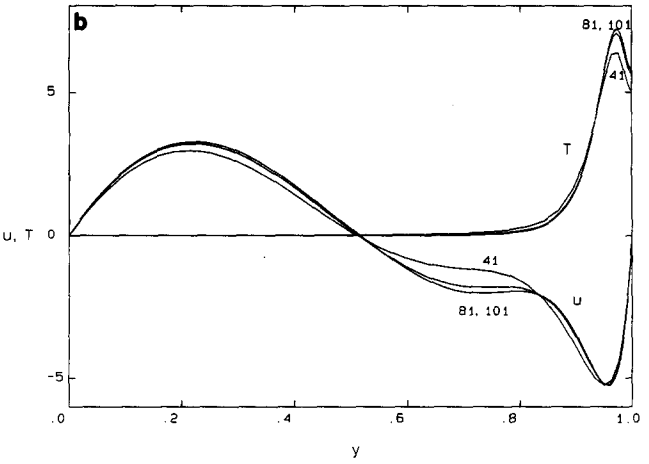

Figure 2b Horizontal component of the velocity (u) and temperature (T) as functions of y for $x = 0.5$ and $t = 0.16$

considered that convergence was attained when the overall sum of the residuals in the mass, momentum, and energy equations was less than 2 percent of the corresponding quantity contained in the integration domain, and the heat balance due to sources and sinks, including the boundaries, was better than 2 percent in steady state.

Results

All results presented in this section were obtained considering $\mathrm{Ra} = 3.9 \times 10^9$ and $\mathrm{Pr} = 224$. The time interval analyzed spans a total of 4.4 nondimensional time units. After this period, the flow pattern is practically equal to that in steady state. In all velocity field figures, the reference vector corresponds to 25 nondimensional velocity units.

Initially, a boundary layer starts developing along the heated wall, and an ascending flow is generated that turns near the top right corner. The fluid enters the boundary layer mostly from the bottom region of the cavity, generating an incipient vortical structure. The corresponding temperature field features a steep horizontal gradient in a thin region close to the hot wall, while the core of the cavity remains isothermal. At this stage, heat is transferred to the cavity mostly by conduction.

At $t = 3.3 \times 10^{-2}$ the velocity field shown in Figure 3a indicates a general acceleration of the flow and a thicker layer

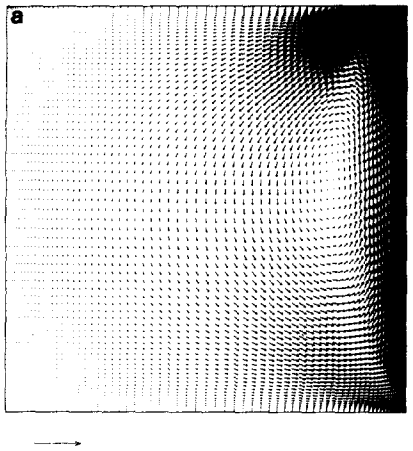

Figure 3a Velocity vectors at $t = 3.3 \times 10^{-2}$. The scale corresponds to 25 nondimensional velocity units

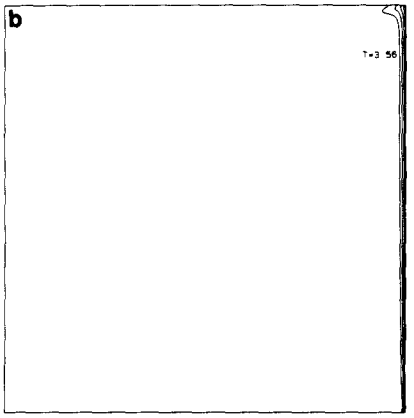

Figure 3b Temperature contours at $t = 3.3 \times 10^{-2}$. The temperatures are multiplied by 10^3, and the difference between consecutive isotherms is 3.56×10^{-3}

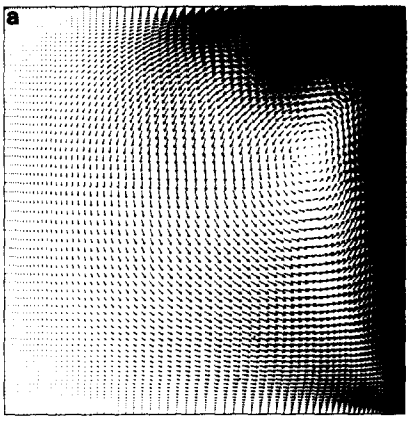

Figure 4a Velocity vectors at $t = 4.9 \times 10^{-2}$. The scale corresponds to 25 nondimensional velocity units

along the heated wall. The vortex in the cavity is clearly formed, and its center is shown to be located at $x = 0.81$, $y = 0.59$. A small temperature gradient starts developing at the upper right-hand corner of the cavity, as can be appreciated from Figure 3b. At 4.9×10^{-2} time units (Figure 4a), the vortex covers a larger part of the cavity, and its center has moved slightly towards the top wall and away from the heated wall to $x = 0.78$, $y = 0.64$. The discharge flow from the boundary layer runs parallel to the top wall and then goes to the core and joins the vortical flow. A nonisothermal region is formed near the upper boundary due to the displacement of the hot fluid from the boundary layer, as shown in Figure 4b; this is the beginning of the intrusion layer.

Figure 5a, obtained at $t = 8.2 \times 10^{-2}$, presents similar features; the vortical structure covers almost the entire cavity,

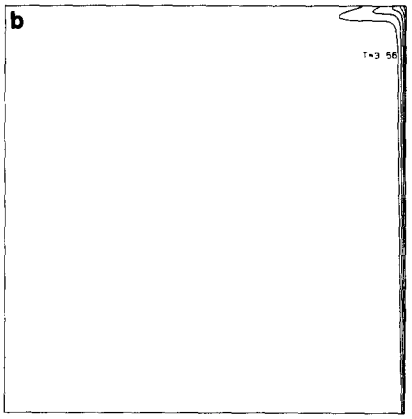

Figure 4b Temperature contours at $t = 4.9 \times 10^{-2}$. The temperatures are multiplied by 10^3 and the difference between consecutive isotherms is 3.56×10^{-3}

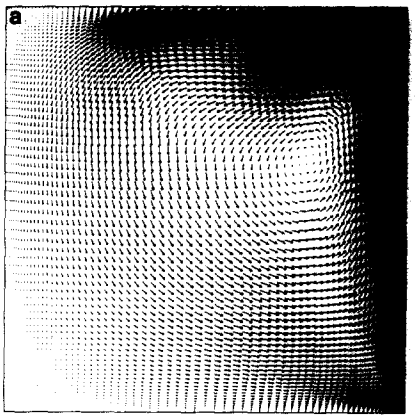

Figure 5a Velocity vectors at $t = 8.2 \times 10^{-2}$. The scale corresponds to 25 nondimensional velocity units

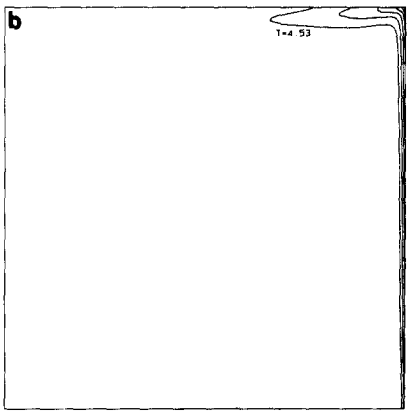

Figure 5b Temperature contours at $t = 8.2 \times 10^{-2}$. The temperatures are multiplied by 10^3, and the difference between consecutive isotherms is 4.53×10^{-3}

and the flow discharged from the boundary layer at the upper part of the cavity forms a thick horizontal stream. The boundary layer is fed through entrainment at a region that extends from the lower wall to approximately three quarters of the cavity height. The thermal boundary layer is now well defined, and hot fluid turns around the corner and forms the intrusion layer that advances towards the constant-temperature wall, as shown in Figure 5b. At $t = 0.16$, the vortex is thinner and its center has moved to $x = 0.80$ and $y = 0.59$ (Figure 6a). It can also be observed from this figure that as the fluid moving parallel to the top wall meets the constant-temperature wall, it starts moving downwards but then turns back to the heated wall. This behavior can be understood by noting that the density of the fluid in the advancing region and in the vicinity of the constant-temperature wall are nearly the same at this stage, since the temperatures are similar (Figure 6b).

Figure 7a ($t = 0.26$) shows that the vortical structure has become thinner in the upper part of the cavity and its center has moved downwards. This results from the interaction of the intrusion layer with the constant-temperature wall and the returning flow. At this time, the hot fluid in the intrusion layer has reached the constant-temperature wall (Figure 7b).

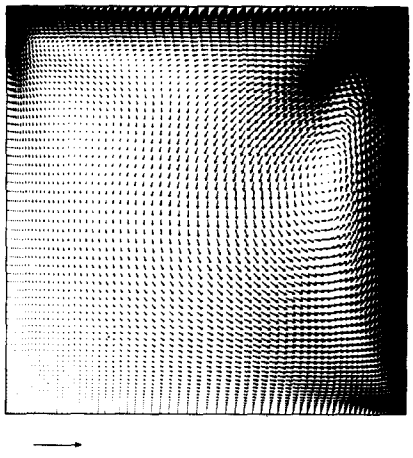

Figure 6a Velocity vectors at $t = 0.16$. The scale corresponds to 25 nondimensional velocity units

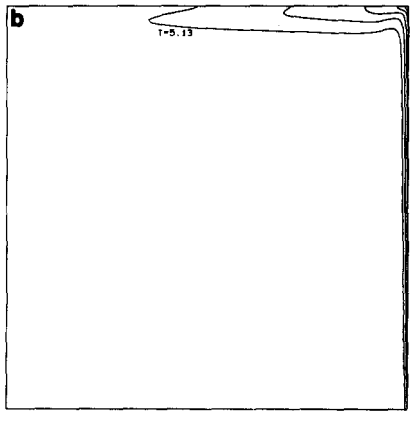

Figure 6b Temperature contours at $t = 0.16$. The temperatures are multiplied by 10^3, and the difference between consecutive isotherms is 5.13×10^{-3}

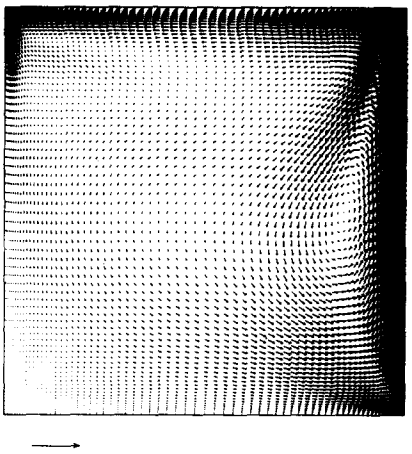

Figure 7a Velocity vectors at $t = 0.26$. The scale corresponds to 25 nondimensional velocity units

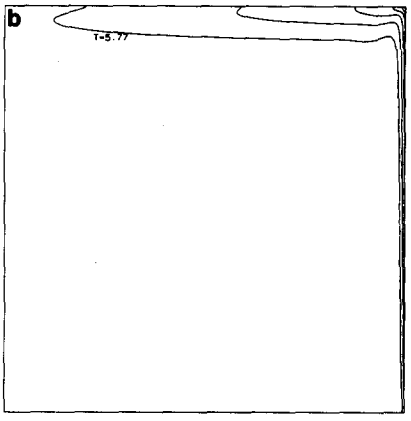

Figure 7b Temperature contours at $t = 0.26$. The temperatures are multiplied by 10^3, and the difference between consecutive isotherms is 5.77×10^{-3}

The velocity field corresponding to $t = 0.69$ (Figure 8a) features an important new effect due to the initial conditions chosen in the study. At previous times, the constant-temperature wall and the fluid in its vicinity are at approximately the same temperature, and therefore no natural convective flow is induced. As time progresses, however, the fluid inside the cavity experiences a net heating, and a thermal gradient is established between the fluid and the constant-temperature wall. This in turn generates a descending boundary layer, as can be observed in Figure 8a. The corresponding temperature field shown in Figure 8b displays the formation of a stratified pattern in the upper region of the cavity.

Finally, at $t = 2.5$ (Figure 9a), the vortical flow near the center of the cavity has disappeared, and the flow is confined to the regions near the walls. The boundary layer near the constant-temperature wall and the intrusion layer along the bottom wall are not as well developed as their counterparts. A more symmetric pattern is obtained at later times when the system has almost reached steady state, as can be seen from Figure 10a, which was obtained at 4.4 time units. Figures 9b and 10b show how the thermal stratification pattern covers the majority of the cavity.

Figures 11a and 11b show the flow and temperature fields obtained by performing the integration without the temporal term in the transport equations. The results at 4.4 time units are very similar to the steady-state solution. It is important to notice that although the boundary conditions are different, the

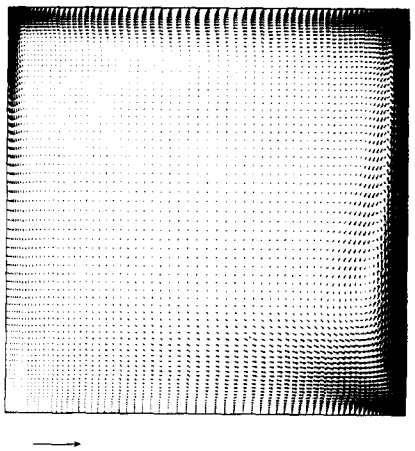

Figure 8a Velocity vectors at $t = 0.69$. The scale corresponds to 25 nondimensional velocity units

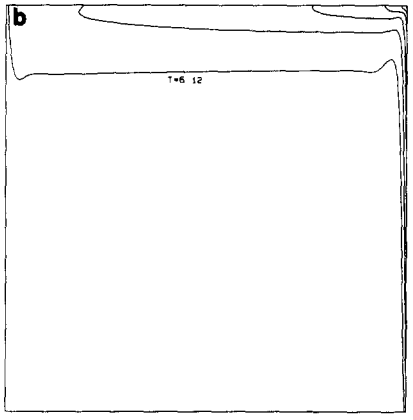

Figure 8b Temperature contours at $t = 0.69$. The temperatures are multiplied by 10^3 and the difference between consecutive isotherms is 6.12×10^{-3}

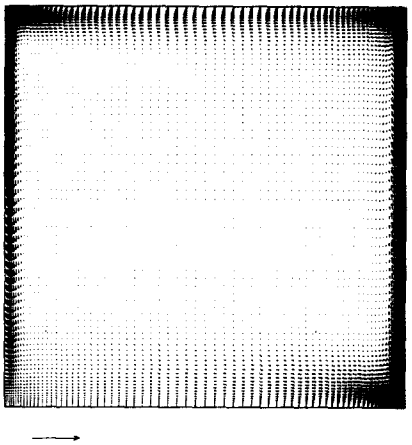

Figure 9a Velocity vectors at $t = 2.5$. The scale corresponds to 25 nondimensional velocity units

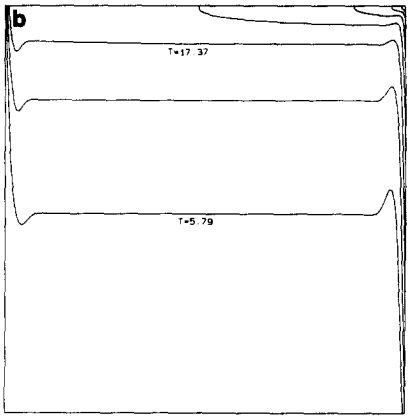

Figure 9b Temperature contours at $t = 2.5$. The temperatures are multiplied by 10^3, and the difference between consecutive isotherms is 5.79×10^{-3}

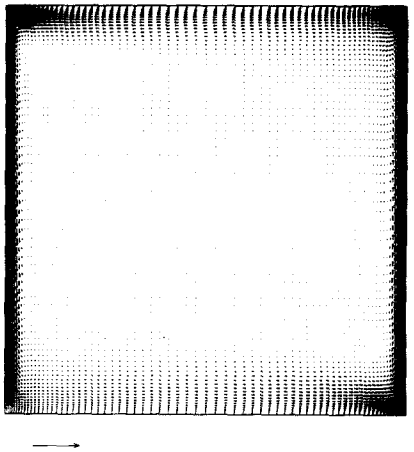

Figure 10a Velocity vectors at $t = 4.4$. The scale corresponds to 25 nondimensional velocity units

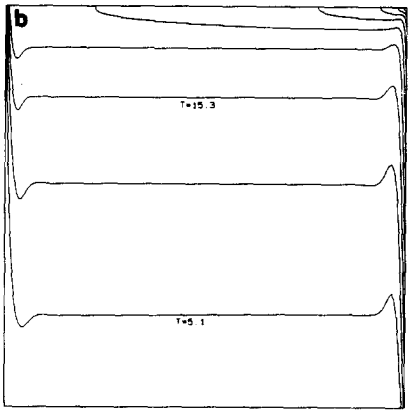

Figure 10b Temperature contours at $t = 4.4$. The temperatures are multiplied by 10^3, and the difference between consecutive isotherms is 5.1×10^{-3}

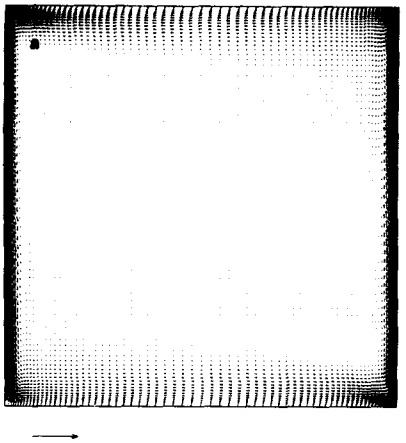

Figure 11a Velocity vectors in steady state. The scale corresponds to 25 nondimensional velocity units

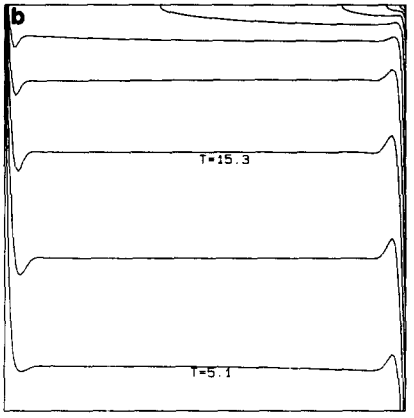

Figure 11b Temperature contours in steady state. The temperatures are multiplied by 10^3, and the difference between consecutive isotherms is 5.1×10^{-3}

flow near the heated and top walls is almost symmetric to that close to the constant-temperature and lower walls. The flow pattern is similar to that obtained by Kimura and Bejan (1984) for constant heat flux in opposite sides of the cavity. A vertical temperature gradient is established in the whole volume. Departures from this behavior are only found near the vertical walls where boundary layers modify the temperature distribution.

Histories of velocities

Figure 12 shows histories of the vertical velocity component (v) near the hot wall (at $x = 0.99$) at different vertical positions. The time scale is logarithmic in order to display clearly the initial behavior. At the higher positions ($y = 0.90$ and $y = 0.75$), the velocity displays a sharp maximum. At the lower positions ($y = 0.10$ and $y = 0.25$), the flow velocity also increases rapidly at the onset of the flow but then decreases slowly to attain its steady state value. At the beginning, all traces (except "e") coincide; subsequently, they diverge. This phenomenon is known in the context of the transient boundary layer on a vertical plate as "the leading-edge effect" (see Gebhart and Mahajan 1982). It should be noted that the maximum velocity is not attained at the highest position ($y = 0.9$) but at $y = 0.75$. This effect is due to the presence of the top wall, which creates an accumulation of pressure near the corner.

The horizontal velocity component for $x = 0.5$ and different vertical positions is shown in Figure 13. As explained below, this figure reflects the global behavior of the flow presented in Figures 2 to 10. Initially an acceleration takes place, and then the vortex motion manifests itself as a damped oscillation with two or three cycles. The origin of these oscillations is different from those predicted by Patterson and Imberger. In fact, the criteria for oscillatory flow in the PI analysis is $Ra_{\Delta T} > Pr^4$ ($Ra > Pr^5$) for the unity aspect ratio, and it is not met in the present case. The PI cavity scale oscillations are produced by horizontal thermal gradients in the intrusion layer and tilting of the isotherms. In the present case, the oscillations are the consequence of the interaction of the vortex structure with the wall, in particular with the upper righ-hand corner, and the returning flow from the intrusion layer. The oscillations take place at the beginning of the flow ($t < 0.2$), before the intrusion layer has reached the constant-temperature wall and therefore when most of the fluid in the cavity is isothermal. These kinds of oscillations have also been found by Hyun and Lee (1989) for similar Prandtl and Rayleigh numbers but with constant wall temperatures on both sides.

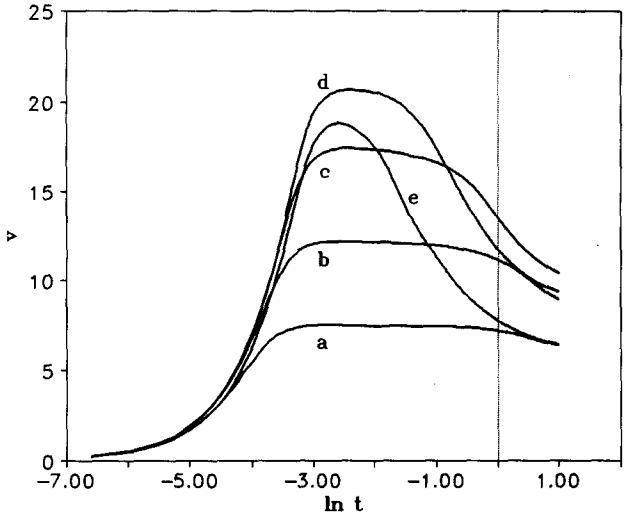

Figure 12 Histories of the vertical velocity component (v) near the hot wall ($x = 0.99$). (a) $y = 0.1$; (b) $y = 0.25$; (c) $y = 0.5$; (d) $y = 0.75$; and (e) $y = 0.9$

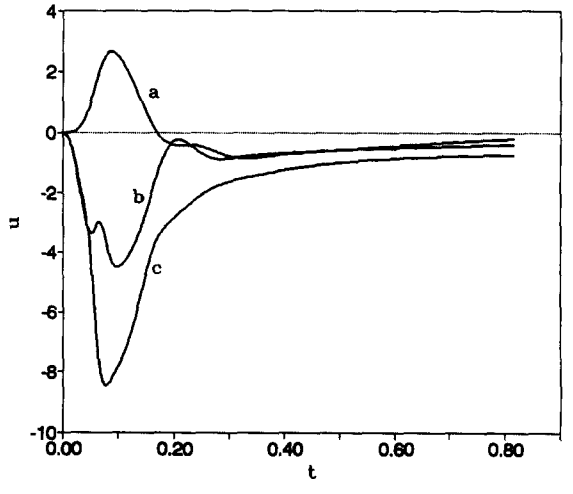

Figure 13 Histories of the horizontal velocity component (u) at $x = 0.5$. (a) $y = 0.5$; (b) $y = 0.75$; and (c) $y = 0.9$

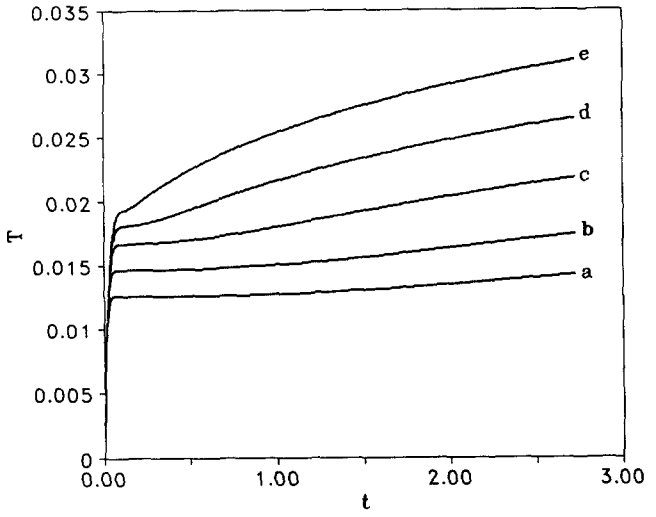

Figure 14 Histories of temperature at the hot wall ($x = 1$). (a) $y = 0.1$; (b) $y = 0.25$; (c) $y = 0.5$; (d) $y = 0.75$; and (e) $y = 0.9$

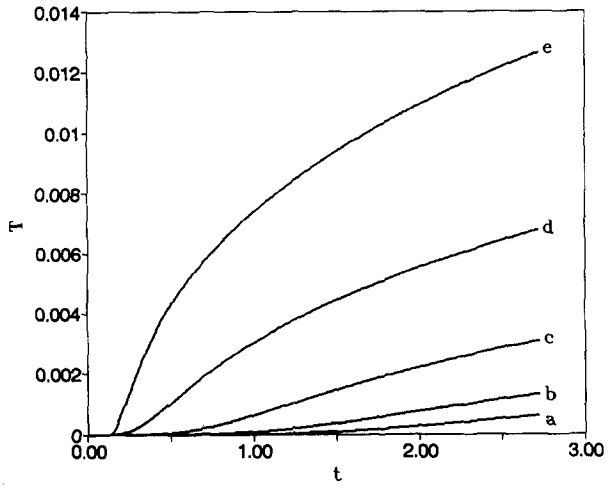

Figure 15 Histories of temperature near the constant-temperature wall ($x = 0.01$). (a) $y = 0.1$; (b) $y = 0.25$; (c) $y = 0.5$; (d) $y = 0.75$; and (e) $y = 0.9$

Histories of temperatures

Figures 14 and 15 show the temperature variation with time at the heated wall ($x = 1.0$) and near the constant-temperature wall ($x = 0.01$), respectively, at five different vertical positions. It can be observed in Figure 14 that initially the temperatures increase monotonically at the same rate for all points; it must be noted that heat transfer takes place mainly by conduction for $t \leq 10^{-2}$. However, higher positions subsequently acquire higher temperatures due to the greater importance of convection in the boundary layer. Eventually, a vertical gradient is established. In Figure 15, it is important to notice that the temperatures do not change immediately after the heating of the cavity has started. The lag reflects the time taken by the hot fluid layer to reach the constant-temperature wall.

Discussion and conclusions

The numerical results obtained in the present investigation have been compared to the scale analysis of Patterson and Imberger, which was modified so that it could be applied for constant heat input conditions (see Appendix for details). Table 1 shows scales according to the two analyses. The agreement is satisfactory, indicating the consistency of the two approaches. Obviously, the nature of the comparisons is qualitative, and in some instances, a range of values is given for the numerical results. The approximate arrival time of the intrusion layer τ_v coincides, in spite of the fact that the Patterson and Imberger analysis assumes a constant mass flow in the thermal boundary layer during the time taken by the intrusion layer to move towards the constant temperature wall, and this is not the case in the present numerical results. The time taken by the fluid to reach steady-state found with the numerical calculation is longer than that of the scale analysis by a factor of two. The reason for this is that in the PI analysis, the thermal boundary conditions on the vertical walls are symmetric and the boundary layers are formed simultaneously; in contrast, in the case studied here, the boundary layer near the constant-temperature wall develops only after the fluid temperature has risen enough to establish a thermal gradient between itself and the constant-temperature wall.

Table 1 Comparison of the Patterson and Imberger modified analysis and the numerical results of the present work

Scales	Patterson and Imberger	Present results
Formation time of boundary layer, τ	3.3×10^{-2}	4×10^{-2}
Thickness of thermal boundary layer, δ_T	1.2×10^{-2}	2.5×10^{-2}
Thickness of viscous boundary layer, δ_v	0.18	(0.15–0.23)
Velocity in the boundary layer, V_T	30	20
Arrival time of the intrusion layer at the constant temperature wall, τ_v	9.8×10^{-2}	1.1×10^{-1}
Thickness of intrusion layer, Δ_T	0.036	0.07
Time to heat the whole volume of fluid, τ_f (filling time)	2.4	>4.4

It is likely that the presence of the vortical flow in the nearly isothermal cavity is due to the high Prandtl number used in the analysis. In these cases, the momentum transfer to the core from the viscous boundary layer is faster than the heat transfer.

The system studied presents four main time scales that are obviously dependent on each other but determined by different physical phenomena. The first scale is given by the formation of the boundary layer adjacent to the constant-heat-input wall ($\sim 4 \times 10^{-2}$); the arrival of the intrusion layer at the constant-temperature wall determines the second (~ 0.1); the third is defined by the presence of the vortical structure (~ 0.7). The fourth time scale is determined by the formation of the boundary layer next to the constant temperature wall, which leads to the steady state (~ 3.5).

Appendix: Adaptation of the Patterson–Imberger scale analysis

In the PI case, where the two vertical walls of the cavity are kept at constant (but different) temperatures, the definition of the Rayleigh number is

$$\mathrm{Ra}_{\Delta T} = \frac{g\beta\Delta T h^3}{\nu\alpha} \tag{A.1}$$

where ΔT is the temperature difference between either wall and the initial fluid temperature. In the present case, a natural definition of the Rayleigh number is

$$\mathrm{Ra} = \frac{g\beta q h^4}{\alpha \nu k} \tag{A.2}$$

It is convenient to define a characteristic temperature difference ΔT^* at the heated wall as follows:

$$\Delta T^* \sim \frac{q\delta_T}{k} \tag{A.3}$$

where δ_T is the thickness of the thermal boundary layer. According to PI analysis, the velocity scale during the formation of the boundary layer is

$$v \sim \frac{g\beta\Delta T t'}{\mathrm{Pr}} \tag{A.4}$$

Using the temperature difference given in Equation A.3 as the characteristic temperature gradient, the velocity scale becomes

$$v \sim \frac{g\beta q \delta_T t'}{\mathrm{Pr}\, k} \tag{A.5}$$

or

$$v \sim \frac{g\beta q \alpha^{1/2} t'^{3/2}}{\mathrm{Pr}\, k} \tag{A.6}$$

Equation A.6 was written using the expression $\delta_T \sim \alpha^{1/2} t'^{1/2}$ from the PI analysis. Once the boundary layer has developed, $\delta_T = h/\mathrm{Ra}_{\Delta T}^{1/4}$. Using this definition and ΔT^*, the following relation is obtained:

$$\mathrm{Ra}_{\Delta T} = \mathrm{Ra}^{4/5} \tag{A.7}$$

The time, thickness, and velocity can then be written in terms of Ra as

$$\tau \sim \frac{h^2}{\alpha \mathrm{Ra}^{2/5}} \tag{A.8}$$

$$\delta_T \sim \frac{h}{\mathrm{Ra}^{1/5}} \tag{A.9}$$

$$V_T \sim \frac{\alpha \mathrm{Ra}^{2/5}}{h} \tag{A.10}$$

In similar form, the arrival time and thickness of the intrusion layer can be expressed as

$$\tau_v \sim \frac{h^2}{\alpha \mathrm{Ra}^{7/20}} \tag{A.11}$$

$$\Delta_v \sim \frac{h}{\mathrm{Ra}^{3/20}} \tag{A.12}$$

References

Armfield, S. W. and Patterson, J. C. 1991. Direct simulation of waves interaction in steady natural convection in a cavity. *Int. J. Heat Mass Transfer*, **34**, 923–940

Gebhart, B. and Mahajan, R. L. 1982. Instability and transition in buoyancy-induced flows. *Adv. Appl. Mech.*, **22**, 231–315

Hyun, J. M. and Lee, J. W. 1989. Numerical solutions for transient natural convection in a square cavity with different sidewall temperatures. *Int. J. Heat Fluid Flow*, **10**, 146–151

Ivey, G. N. 1984. Experiments on transient natural convection in a cavity. *J. Fluid Mech.*, **144**, 389–401

Kimura, S. and Bejan, A. 1984. The boundary layer natural convection regime in a rectangular cavity with uniform heat flux from the side. *Trans. ASME, J. Heat Transfer*, **106**, 98–103

Patankar, S. V. 1980. *Numerical Heat Transfer and Fluid Flow*. Hemisphere/McGraw Hill, Washington

Patterson, J. C. 1984. On the existence of an oscillatory approach to steady natural convection in cavities. *Trans. ASME, J. Heat Transfer*, **106**, 104–108

Patterson, J. C. and Armfield, S. W. 1990. Transient features of natural convection in a cavity. *J. Fluid Mech.*, **219**, 469–497

Patterson, J. C. and Imberger, J. 1980. Unsteady natural convection in a rectangular cavity. *J. Fluid Mech.*, **100**, 65–86

Paolucci, S. 1990. Direct numerical simulation of two-dimensional turbulent natural convection in an enclosed cavity. *J. Fluid Mech.*, **215**, 229–262

Paolucci S. and Chenoweth, D. R. 1989. Transition to chaos in a differentially heated cavity. *J. Fluid Mech.*, **201**, 379–410

Schladow, S. G. 1990. Oscillatory motion in a side heated cavity. *J. Fluid Mech.*, **213**, 589–610

Schladow, S. G., Patterson, J. C., and Street, R. L. 1989. Transient flow in a side heated cavity at high Rayleigh number: a numerical study. *J. Fluid Mech.*, **200**, 121–148

Yewell, R., Poulikakos, D. and Bejan A. 1982. Transient natural convection experiments in shallow enclosures. *Trans. ASME J. Heat Transfer*, **104**, 533–538